Type of the Paper: Article

Reuse of electrocoagulated metal hydroxide sludge to fluoride and arsenic removal by a fixed-bed column in continuous operation

C. García-Gómez[1,2], M.L. Rivera-Huerta[3], F. Almazán-García[3], A. Martín-Domínguez[3], V.A. Burboa-Charis[e2], I.C. Romero-Soto[2], R. G. Ulloa-Mercado[2], D. Serrano-Palacios[2], P. Gortáres-Moroyoqui[2]

[1]Universidad Autónoma de Nuevo León (UANL), Facultad de Agronomía, Francisco Villa S/N, C. P. 66050 General Escobedo, Nuevo León, México.

[2] Instituto Tecnológico de Sonora (ITSON), Departamento de Biotecnología y Ciencias Alimentarias, 5 de Febrero 818 Sur C.P. 85000 Cuidad Obregón, Sonora, México.

[3]Instituto Mexicano de Tecnología del Agua (IMTA), Paseo Cuauhnahuac 8532 Progreso C.P. 62550, Jiutepec, Morelos, México.

* Correspondence: pablo.gortares@itson.edu.mx; Tel.: +52 644 4109000 ext. 2110

Featured Application: The work provides a fundamental understanding on the removal of fluoride and arsenic through the Reuse of electrocoagulated metal hydroxide sludge. Fixed-bed column experiments using a response surface methodology were performed to investigate the effect of column parameters. This kind of experimental design gives a depth understanding for the design of fixed-bed adsorption processes to facilitate scaling up of the processes.

Abstract: In the present study, Electrocoagulated Metal Hydroxide Sludge (EMHS) was analyzed as adsorbent material to remove both fluoride ion (F-) and arsenic V (As(V)) from aqueous effluents. This material was generated during an electrocoagulation process using Aluminum anode. It was characterized by using specific surface areas and the surface morphology was studied by scanning electron microscopy (SEM). Adsorbent fixed-beds are generally studied to remove different class of contaminants. EMHS was evaluated using a continuous flow rate column test with an experimental design. The effect of initial concentration of F- (2.5-10 mg L^{-1}) and the Empty Bed Contact Time (EBCT (0.4-0.8 min)) was studied following a central composite design methodology. The experimented parameters had a significant influence on saturation time, breakthrough volume, and breakthrough time. A response surface analysis was a tool for analyzing the adsorption study, showing interactions that are complicated to identify by others methods. The results, here reported, revealed that EMHS is an efficient and promising adsorbent material in order to remove F- and As(V) from water contaminated by these pollutants.

Keywords: Fixed-bed column, fluoride, arsenic, removal, response surface methodology

1. Introduction

The expanded distribution of diverse ionic elements such as fluoride and arsenic in water as result of diverse industry process or naturally occurring has generated interest from the scientific researches since they are affecting human health in the world. In this context, the most substantial inorganic pollutants in groundwater, stablished by the World Health Organization (WHO), are fluoride (F^-) and arsenic (As) [1].

 doi:10.20944/preprints201809.0537.v1

F^- at small amount is favorable for bone and teeth development, but in concentrations elevated are harmful to human health, provoking skeletal or dental fluorosis [2]. On the other hand, As is distinguished for generate cancer in skin, lung, kidney, liver and bladder, besides gastrointestinal problems and arsenicosis [3]. Therefore, the WHO recommends guideline values for F^- and As concentrations with the upper permissible limit in water of 1.5 mg L^{-1} and 10 μg L^{-1}, respectively [4]. In many places worldwide, F^- and As concentrations show a significant co-contamination in groundwaters whit concentrations up of 29 mg L^{-1} and 5300 μg L^{-1} for F^- and As, respectively [5]. In the actuality water contaminated with F^- and As is a concern, which requires an efficient treatment. In the literature several strategies have been put in practice to perform the F^- and As removal from water, for F^- strategies as chemical precipitation/coagulation [6], electrocoagulation and electrocoagulation/flotation [7, 8], adsorption [9, 10] ion exchange [11, 12] reverse osmosis and nanofiltration [13], and electrodialysis [14, 15]. The most technologies frequently used for As removal can be used for F^- removal, to be specific, chemical methods [16], adsorption [17, 18] , Ion exchange [19], membrane technology [20]. These strategies has its own advantages and disadvantages with removal efficiencies ranging from 60% until 100%.

Adsorption technique has shown considerable potential due to its simplicity, chemicals addition are not necessary, and its efficiency with high grade of total solids [21]. Different strategies has been used employing diverse materials for individual and concurrent elimination of F^- and As. Several adsorbents have been used to eliminate F^- and As in both, individual and a concurrent way such as activated carbon [22], layered double hydroxides [23], aluminum hydroxide [24], ferric hydroxide [25], goethite [26], Fe-Ce oxides [20], Fe-Al doped polymers [27], Haix-Fe-Zr and Haix-Zr resin beads [28], inorganic ion exchange adsorbents [29], mesoporous aluminas [30], modified cellulose [31] and volcanic ash [32] Researches are looking simple and cost effective processes, diverse low cost materials from different sources have been applied for F^- and/or As removal [33].

A candidate strategy for providing low-cost adsorbent can be Electrocoagulated Metal Hydroxide Sludge (EMHS) which is obtained from an electrocoagulation (EC) system, in this process sacrificial aluminum or iron electrodes are oxidized releasing hydroxides of these metals. Metallic hydroxides can separate some pollutants by electrostatic attraction or surface complexation [34]. The disposal of these materials, which is considered as waste, are actually a critical subject because they can cause environmental and public health impacts without an appropriate management [35]. The EMHS can be utilized to remove F^- and As from the effluents which formed the motivation of this study.

In this investigation, EMHS was reused before disposal for a modelling and experimental research. No results of fluoride and arsenic removal in fixed bed coulum by EMHS have been presented so far. Therefore, the overall motivation for investigating the effect of this molecules on sorption is toward developing a mechanistic understanding of inorganic sorbate–EMHS interactions. The characteristics of EMHS using specific surface areas and scanning electron microscopy techniques were analyzed. The influence of column variables such as empty bed contact time (EBCT) and fluoride ion (F^-) concentration in a continuous flow fixed-bed column have been investigated using a response surface methodology.

2. Materials and Methods

2.1. Chemicals and analytical method

All of the reagents used in this work were analytical grade and were used without any further purification. Fluoride (F^-) and arsenic (As(V)) stock solutions were made from sodium fluoride (NaF) and sodium arsenate ($NaAsO_3 \cdot 12H_2O$), respectively. Hydrochloric acid (HCl) and sodium hydroxide (NaOH) were used to adjust requiered pH. Fluoride concentration was monitored using an ion-selective electrode for fluoride ion (Thermo Scientific 9609 BNWP), while for As concentration a digital arsenic Test Kit (Arsenator®) was used.

 doi:10.20944/preprints201809.0537.v1

2.2 Adsorbent material preparation

EMHS applied to adsorption research and carried out in this investigation was by-produced from electrocoagulation (EC) pilot plant using aluminum anodes, at the say way as is reported in a previous work [36]. A flow diagram of the adsorbent by-production used in this study is shown on Fig 1.

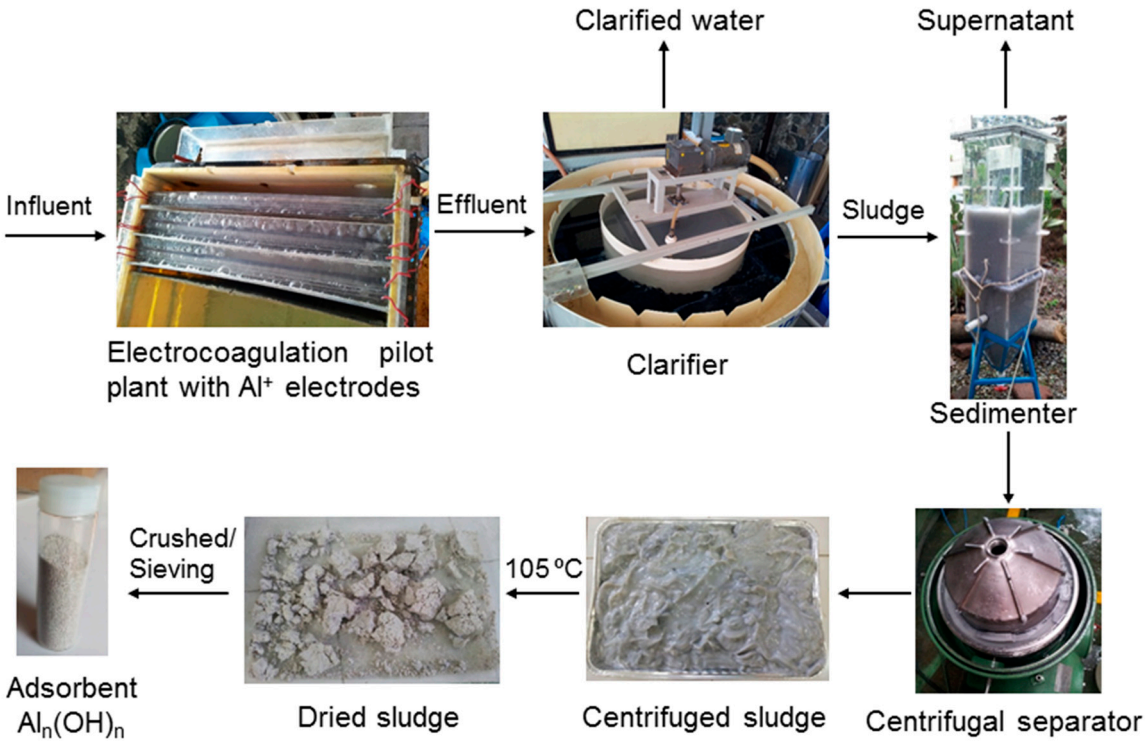

Figure 1. Process flow diagram of the EMHS production.

2.3. Material characterization

The characterization of EMHS was analyzed by N_2 adsorption–desorption isotherms at 76 K utilizing a Micromeritics ASAP 2020 surface area and porosity analyzer. N_2 isotherms with the Brunauer–Emmett–Teller method (BET) was used to determine the surface area BET. The volume of liquid nitrogen corresponding to the amount adsorbed at relative pressure of $P/P_0 = 0.99$ and was defined as the total pore volume, V_T. The Dubinin–Radushkevich method was used to determine the micropore volume, $V\mu$, and the mesopore volume, V_m, was obtained with the difference between V_T and V_μ. The average pore diameter, D_p, was calculated using the relation $4\ V_T$ /area BET and the pore size distribution by Density–Functional–Theory method (DFT). The scanning electron microscopy (SEM) assay was carried out for the adsorbent material in order to analyze their morphology.

2.4. Column studies

Adsorption processes design in a full scale involves a lot of time and expensive pilot plant evaluations. These experiments could take several years. For prevent these expensive studies quick laboratory experiments are employed. The small-scale fixed bed column test is, possibly the most useful tool to evaluate adsorbents capacity to remove pollutants. In a series of column test were studied the influence of the initial F^- concentration (mg L^{-1}) and empty bed contact time (EBCT, (min)). According to several investigations [37], a prediction of the variation of adsorption contaminants rate on adsorbents as adsorbate concentration is difficult. If intraparticle diffusion is the main mechanism, an equilibrium interfacial concentration should form rapidly that is followed by slow diffusion into the adsorbent particles. Then, a simple dependence on solution concentration is not expected. Moreover, the mathematical treatment of intraparticle diffusion does not lead a simple algebraic relationship between external solute concentration and time of reaction even when a constant

Preprints (www.preprints.org) | NOT PEER-REVIEWED | Posted: 27 September 2018 doi:10.20944/preprints201809.0537.v1

saturated external layer is maintained. In this case, concentration effect is used to define the rate-limiting reaction step. When intraparticle transport limits the kinetic of an adsorption reaction, the variation in reaction rate is not expected to be linear, whereas the rates of strictly adsorptive reactions and simple diffusion-controlled processes are expected to be proportional to the of adsorbate´s concetration.

Arsenic concentration was fixed at 100 μg L^{-1}. The EBCT is represented by the flow rate through the column, this parameter influences the shape of breakthrough curve and the volume to breakthrough. The EBCT is resolved using equation (1):

$$\text{EBCT (min)} = \frac{\text{bed volume (cm}^3\text{)}}{\text{volumetric flow rate } \left(\text{cm}^3\ \text{min}^{-1}\right)} \quad (1)$$

An acrylic column of 2 cm internal diameter and 100 cm length was filled with metal hydroxide sludge as adsorbent. Before to start column tests, a flow rate of 26 ml min^{-1} of deionized water was introduced in the column for 5 min with the propose of remove air bubbles and to guarantee a closely packed disposal of particles without cracks, channels or voids. After that, the pollutant solution was passed through a fixed-bed of adsorbent in down-flow mode. A flow rate of 26 ml min^{-1} was controlled with a peristaltic pump. Periodically, samples were collected from the effluent and then analyzed for the remaining pollutant concentration. Temperature was maintained around 21±0.8ºC, while pH of the medium was fixed at 7 in all experiments.

2.5. Experimental design

The one variable at a time or step-by-step variable strategy is the traditional way to analyzed the effect of several independent variables or factors over dependent variables or response variables, in which the variables remain constants and only one is changing. However, this strategy implicates several number of runs and interactions among factors are missed. These drawbacks can be solved by response surface methodology (RSM). This methodology is a mathematical and statistical method functional for studying and optimizing processes [37]. Therefore, for explore the impact of operating conditions on diverse process the RSM can be an alternative. The Central Composite Design (CCD) methodology is commonly used class of second-order designs. It implicates the use of a two-level factorial design with $\boldsymbol{2^k}$ points combined with $\boldsymbol{2 * k}$ axial points and $\boldsymbol{n}$ center runs, where $\boldsymbol{k}$ being the number of factors experimental. The total number of experiments $\boldsymbol{N}$, with $\boldsymbol{k}$ factors experimental is (Eq. (2)):

$$\boldsymbol{N = 2^k + 2 * k + n} \quad (2)$$

Figure 3 shows the coded presentation of the CCD for 2 factors.

Factorial designs with two levels (2^K) have advantage in the total of experimental runs compared with the 'one variable at a time' method. Here a mathematical model can be used to define the behavior of the response variable on the interest zone. In this investigation a RSM was developed based on the CCD methodology experiments.

The statistical software of Design-Expert (version 7.0, STAT-EASE Inc., Minneapolis, MN, USA) was applied for designing and analyzing the experimental results. The values of process variables and their variation limits were selected based on the preliminary experiments. For statistical purposes, the transformation of independent variables ($\boldsymbol{X_i}$) into coded corresponding variables ($\boldsymbol{x_i}$) was generated by (Eq. (3)):

$$\boldsymbol{x_i = \frac{(X_i - X_0)}{\Delta X}} \quad (3)$$

Where $\boldsymbol{X_0}$ is the value of $\boldsymbol{X_i}$ at the center point and $\boldsymbol{\Delta X}$ represents the step change. The table 1 shows the codified levels. ANOVA was applied to RSM model to study the individual and combined effect of two variables X_1 and X_2. The response variables studied were related with F^- pollutant like saturation time ($\boldsymbol{t_s}$), breakthrough volume ($\boldsymbol{V_b}$), and breakthrough time ($\boldsymbol{t_b}$). Also, arsenic removal efficiency (% of removal) is reported. The sequential model fitting test was implemented in order to select an appropriate model. For express the response variable in the investigated domain it is

Preprints (www.preprints.org) | NOT PEER-REVIEWED | Posted: 27 September 2018 doi:10.20944/preprints201809.0537.v1

appropriate an adjustment for a mathematical model equation. Generally, to describing a flat surface the first-order model can be used under to the following expression (Eq. (4)):

$$\mathbf{Y} = \boldsymbol{b_0} + \sum \boldsymbol{b_i x_i} \quad (4)$$

Where $\mathbf{Y}$ is the response variable, $\mathbf{b_0}$ is the constant coefficient, $\boldsymbol{b_i}$ represents the coefficients of the linear parameters, $\boldsymbol{x_i}$ represents the variables studied. When interaction terms are incorporated (FI model or factor interactions), the next equation (Eq. (5)) can represent the first-order model:

$$\mathbf{Y} = \boldsymbol{b_0} + \sum \boldsymbol{b_i x_i} + \sum \boldsymbol{b_{ij} x_i x_j} \quad (5)$$

Where $\boldsymbol{b_{ij}}$ represents the coefficients of the interaction parameters $\boldsymbol{x_i}$ and $\boldsymbol{x_j}$ and $\boldsymbol{i < j}$.

Table 1. Experimental range and level of independent variables.

		Experimental field				
Independent variables	Factor	$-\alpha$ ($-\sqrt{2}$)	Low (-1)	Middle (0)	High (1)	$+\alpha$ ($\sqrt{2}$)
F^- concentration (mg L^{-1})	X_1	0.94	2.5	6.25	10	11.55
EBCT (min)	X_2	0.31	0.4	0.6	0.8	0.88

Sometimes for an interpretation of relationships with independent variables the FI or first-order models are not convenient. For this reason, a more highly diversified, structured and flexible model like a second-order model can be applied and this way establish the optimum value. The second-order model can be predicted by the following equation (Eq. (6)):

$$\mathbf{Y} = \boldsymbol{b_0} + \sum \boldsymbol{b_i x_i} + \sum \boldsymbol{b_{ij} x_i x_j} + \boldsymbol{b_{ii} x_i^2} \quad (6)$$

where $\boldsymbol{b_{ii}}$ expresses the coefficients of the quadratic parameter and $\boldsymbol{i < j}$.

An experiment can be optimized for examining the analysis of variance (ANOVA) statistics (R^2, the adjusted R^2, lack-of-fit, F-test and t-test), the residual analysis, normal plots, interaction effects and the contour plot, and this way decide the fit of the first-order or second-order model. The runs carried out are shown in Table 2.

Table 2. Central composite design analysis: experimental conditions and results.

Experiment plan		Response variables		
X_1 (mg L^{-1})	X_2 (min)	t_b (min)	V_b (L g^{-1})	t_s (min)
0.4	2.5	65	0.330	817
0.4	10	36	0.178	600
0.8	2.5	233	0.585	1242
0.8	10	122	0.336	1116
0.317	6.25	22	0.152	540
0.6	0.946	184	0.543	1440
0.882	6.25	134	0.385	1080
0.6	11.556	33	0.121	600
0.6	6.25	122	0.348	1140
0.6	6.25	98	0.360	1240
0.6	6.25	85	0.312	1220

 doi:10.20944/preprints201809.0537.v1

193 *2.6. Optimization: Desirability function.*
194 The desirability is a multiple response method, which is useful for the process optimization. This
195 method utilizes an objective function or desirability function (D), which change a calculated response
196 into a value from zero to one, in other words, form least to most desirable. The optimal parameter
197 conditions are considered with maximum desirability. The desirability function is maximized by the
198 numerical optimization. Regulating the importance may change the attribute of a goal. The
199 desirability function combines all goals of several responses. In the optimization, both the
200 independent and response variables have a low and high value for every goal.
201
202 **3. Results**
203 *3.1. Characterization*
204 3.1.1. SEM analysis
205 Micrograph obtained from EMHS is shown in Fig. 2, where the morphology of the sample
206 presents particle sizes between 5 and 350 micrometers. In general, the adsorbent studied showed a
207 brightness in the regions analyzed, which indicates chemical consistency related to C, Si, O, and Al.

Preprints (www.preprints.org) | NOT PEER-REVIEWED | Posted: 27 September 2018 doi:10.20944/preprints201809.0537.v1

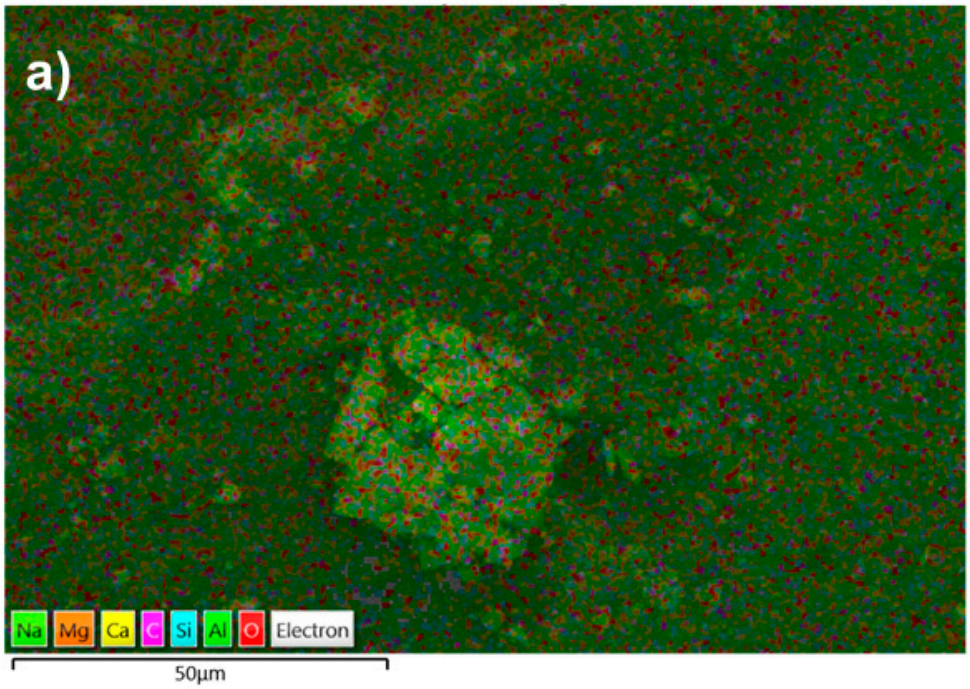

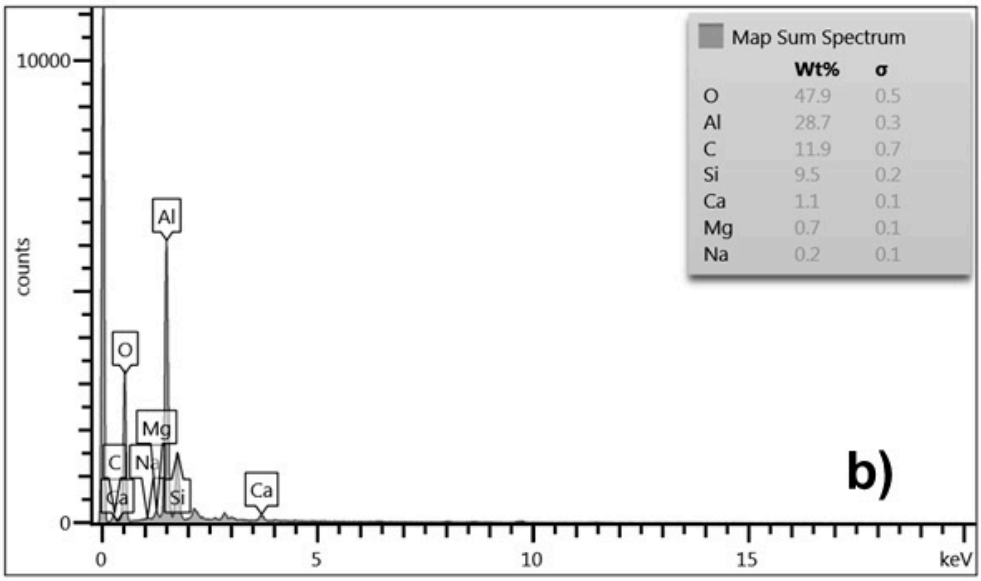

Figure 2. SEM micrographs of EMHS: a) 3 mm reference scale, and b) 500 µm reference scale.

3.1.2. N_2 adsorption–desorption and pore size distribution.

Nitrogen adsorption-desorption isotherm and the BJH pore size distribution of EMHS are shown in Fig. 3. Usually, pores are classified according on the diameter as macropores (d > 50nm), mesoporous (2 nm < d < 50 nm) and microporous (d < 2 nm). As can be seen in Fig. 3a, according the average pore diameter of EMHS comprised mesopores and macropore, given that diameter is within the range of 2–50 nm and partially more than 50 nm. The result can be confirmed by the nitrogen adsorption/desorption isotherms in Fig. 3b. It can be seen that EMHS exhibited an IV type N_2 adsorption isotherm with an evident hysteresis loop (according to the IUPAC classification), implying the existence of mesopores structures in the material [39]. Furthermore, the existence of macropores is evidenced given that the hysteresis loop shifts approach relative pressure (p/p0)=1.

Preprints (www.preprints.org) | NOT PEER-REVIEWED | Posted: 27 September 2018 doi:10.20944/preprints201809.0537.v1

The adsorbent showed a total pore volume (TPV) of 0.76 $cm^3\ g^{-1}$ and a BET surface area of 350.19 $m^2\ g^{-1}$. From the TPV amount, only 0.007 $cm^3\ g^{-1}$ is due to the micropore volume, and 0.753 $cm^3\ g^{-1}$ correspond to mesopore volume. In other words, the EMHS is composed mainly of mesopores and macropores (99%). According to the DFT and BET analysis, the average pore width was 8.43 nm. A large adsorption capacity of the EMHS is confirmed due to high porosity, small pore structures and large specific surface area, indicating its potential as adsorbent.

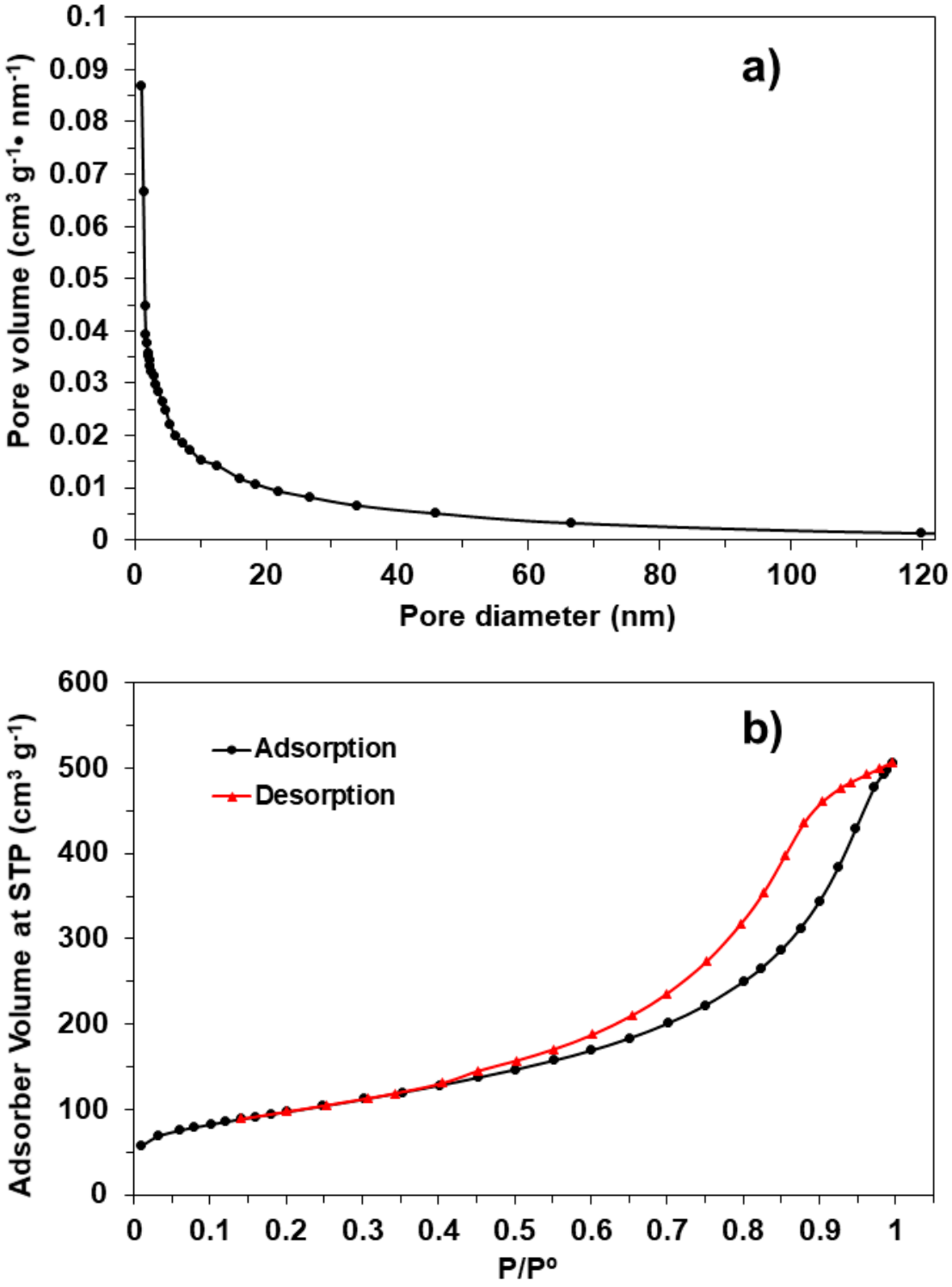

Figure 3. Nitrogen adsorption-desorption isotherm (a) and the BJH pore-size distribution curve (b) of the obtained EMHS.

 doi:10.20944/preprints201809.0537.v1

230
231 3.1.3. Column studies
232 The most significant conditions, which impact in the performance of pollutant removal in a
233 column adsorption method, are initial pollutant concentration and EBCT. Experiments were carry
234 out for varied interactions of the operational parameters using a design of experiments and this way
235 explore the effects of factors mentioned above. For obtain the regression equations were fitted to the
236 experimental data a linear, interactive, quadratic and cubic models. Two different tests were carried
237 out to represent by models the F^- performance in function of the response variables (t_b, V_b, t_s) by
238 EMHS, from the sequential model sum of squares and model summary statistics, cubic model was
239 aliased. The linear model showed a *p*-value was less of 0.01 on all response variables (data not shown),
240 according to sequential model sum of squares. Model summary statistics showed that the excluding
241 cubic model which was aliased, lineal model was found to have maximum ''adjusted R-Squared''
242 and the ''Predicted R-squared'' values on all response variables. For that reason, lineal model was
243 selected for statistical analysis.
244 ANOVA method was utilized to verify the fitness as well as the significance of the models. In
245 our ANOVA results (data not shown), the model *F*-values of 24.57, 38.62 and 8.57 implied that the
246 model is significant for $\boldsymbol{t_b}$, $\boldsymbol{V_b}$ and t_s, respectively also there was only a 0.04%, 0.01% and 1% chance
247 that a model F-value could occur due to noise. A Prob F under 0.05 suggested that model terms are
248 significant. A lack of fit F^- value of 2.51, 5.05 and 17.90 implied the lack of fit is not significant relative
249 to the pure error and there is a 31.24%, 17.42% and 5.48% chance that a lack of fit F-value this large
250 could occur due to noise for $\boldsymbol{t_b}$, $\boldsymbol{V_b}$ and t_s, respectively. Given that we want the model to fit, non-
251 significant lack of fit is necessary.
252 Predicted R^2 is an indicator of how the model forecast a response variable. Both, predicted R^2
253 and adjusted R^2 should be near (no more of 0.20) to be a permissible adjustment, if not the
254 experimentation has a problem with the data. In our case, for all response variables the predicted R^2
255 is near with the adjusted R^2. A signal to noise ratio or in other words a range in estimated response
256 in relation to its error is called adequate precision, where must be at least 4 its desired value. A value
257 of 16.647 indicated an acceptable signal in our experiments. In this model, the coefficient of variation
258 can represent the error, declared as a percentage of the mean. In addition, for verify the significance
259 over the coefficients the P-values were utilized, which also indicate the way of the interactions
260 between the variables. With small values of P, the coefficient is more significant. From our results the
261 coefficients A and B (for F^- concentration and EBCT, respectively) were significant, with small P-
262 values ($P < 0.05$) (data not shown).
263 The results were also examined to verify the normality of the residuals. The normality of the
264 data can be identifying with a normal probability plot, this is a strategy for calculate if a data group
265 is normally distributed [40]. The difference between the predicted and the real value is called residual.
266 If the data are normally distributed, the values should be located on the plot close to the straight line.
267 In our results the data points were reasonably aligned with a straight line (data not shown),
268 suggesting normal distribution for the three variables of response. Fig. 4 represents the predicted and
269 actual values of the response variables for the removal of fluoride onto EMH. The developed model
270 is adequate for all response variables in view the prediction residuals from the responses are
271 distributed in a diagonal line.

Preprints (www.preprints.org) | NOT PEER-REVIEWED | Posted: 27 September 2018 doi:10.20944/preprints201809.0537.v1

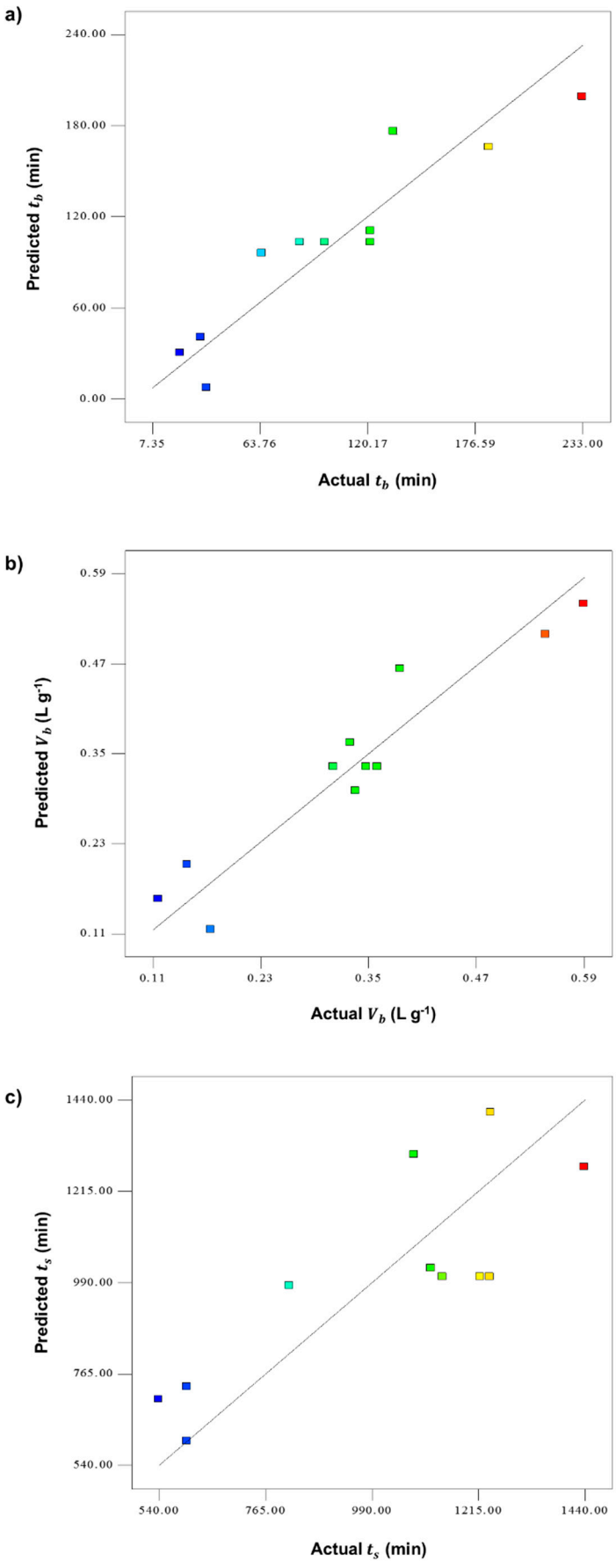

Figure. 4. Predicted response versus actual response for response variables: a) t_b, b) V_b and c) t_s.

Preprints (www.preprints.org) | NOT PEER-REVIEWED | Posted: 27 September 2018 doi:10.20944/preprints201809.0537.v1

During the experiments the pH in the effluent was increasing from pH of 7 to 7.8 in all experiments. This results implies that the OH^- ions were released in the effluent during the experimentation. A breakthrough curve obtained in this work is shown in Fig. 5. In overall view, all samples exhibited the adsorption type I isotherm, which is a characteristic of materials predominantly having micropores.

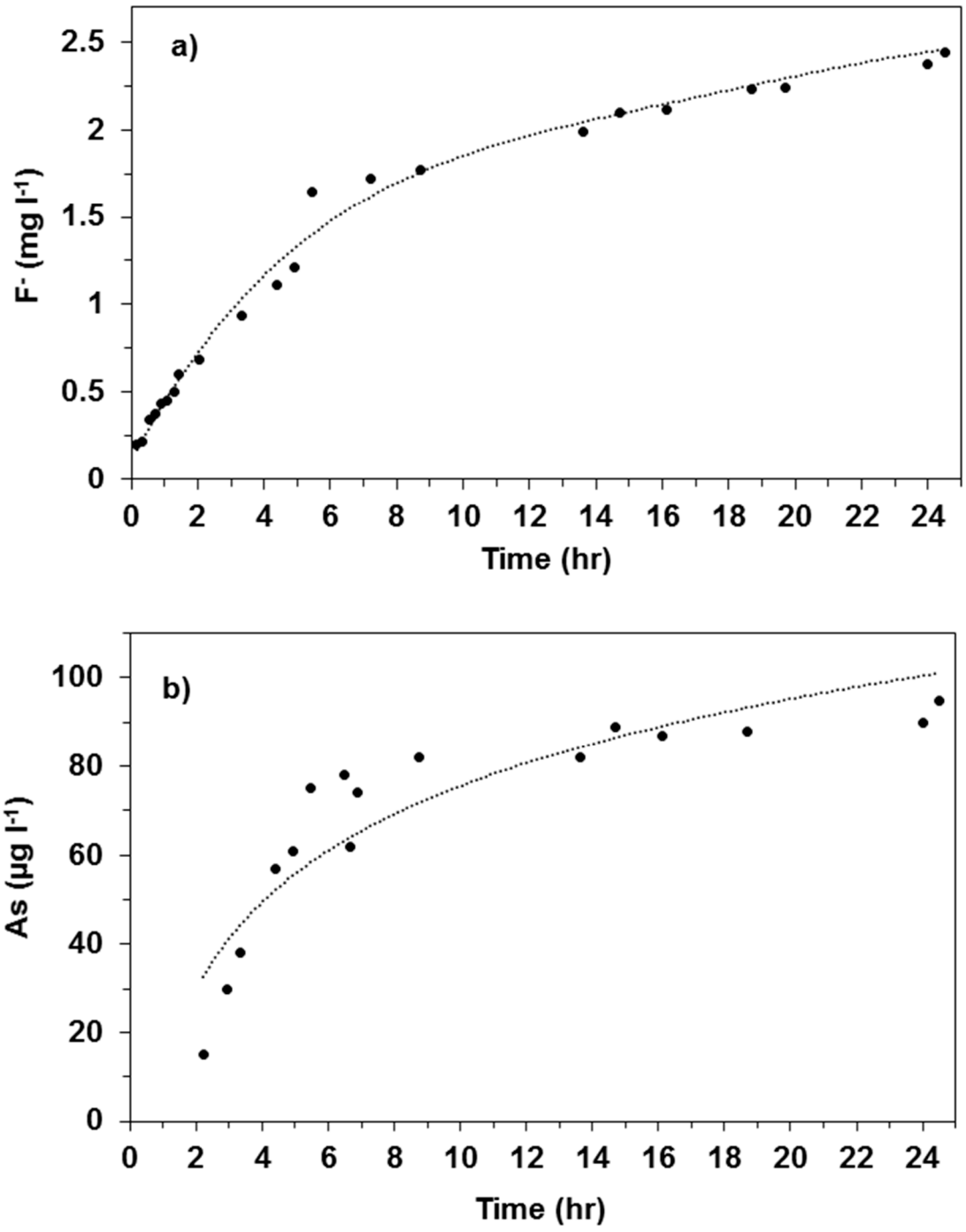

Figure 5. Example of the breakthrough curve by (a) F^- and (b) As using F^- concentration=2.5 mg L^{-1}, EBCT=0.8 min and As concentration= 100 µg L^{-1}.

Preprints (www.preprints.org) | NOT PEER-REVIEWED | Posted: 27 September 2018 doi:10.20944/preprints201809.0537.v1

Table 2 shows the independent and dependent variables used and the results obtained in this study. Breakthrough time was the primary parameter estimated ($\mathbf{t_b}$), which is the time required for 50% of adsorbent saturation. The application of the model in terms of coded factors to the results generated the following equation (Eq. (7)):

$$\mathbf{t_b = 103.09 - 44.19X_1 + 55.51X_2} \quad (7)$$

The $\boldsymbol{r^2}$ value shows high correlation between the model (Eq 7) and the experimental data. In other words, the experimental data fit the model very well. Figure 6 plots the corresponding response surface. Both F^- concentration and EBCT have a significant effect on $\mathbf{t_b}$, which increases with high values of EBCT and when F^- concentration decrease.

For estimate the volume of influent treated by gram of adsorbent ($\boldsymbol{V_b}$), the equation 8 can be used:

$$\boldsymbol{V_b = \frac{v_t}{m_a}} \quad (8)$$

Where $\boldsymbol{v_t}$ is the volume of treated influent and $\boldsymbol{m_a}$ is the mass of dry adsorbent used. The resulting quadratic model is (Eq. (9)):

$$\mathbf{V_b = 0.33 - 0.12X_1 + 0.093X_2} \quad (9)$$

Figure 7 shows that $\mathbf{V_b}$ is in function of F^- concentration and EBCT. $\mathbf{V_b}$ increase at the maximum in the region between 2.5 and 4 mg L^{-1} of F^- and between 0.7 and 0.8 min for EBCT.

The time required to saturate (saturation time, $\mathbf{t_s}$) the adsorbent is one of the most important variable used to describe the performance of an adsorption process. This time is when outlet concentration is equal to $\boldsymbol{C_O}$. The selected breakthrough concentration was fixed at 10% of the inlet feed concentration. The quadratic model found for $\mathbf{t_b}$ is (Eq. (10)):

$$\mathbf{t_s = 1003.18 - 191.37X_1 + 213.08X_2} \quad (10)$$

In contrast to the other response variables, the effect of both independent variables, F^- concentration and EBCT on saturation time (t_s) is not independent of each other, but there is a synergistic effect among independent variables. The zone where F^- concentration and EBCT variables are highest represent the highest t_s values (Fig. 8). According to the results obtained in this investigation, the Surface Response Methodology can be applied in to study adsorption investigations, because of interactions or synergistic effects among independent variables not can be examined by the traditional step-by step methods.

Preprints (www.preprints.org) | NOT PEER-REVIEWED | Posted: 27 September 2018 doi:10.20944/preprints201809.0537.v1

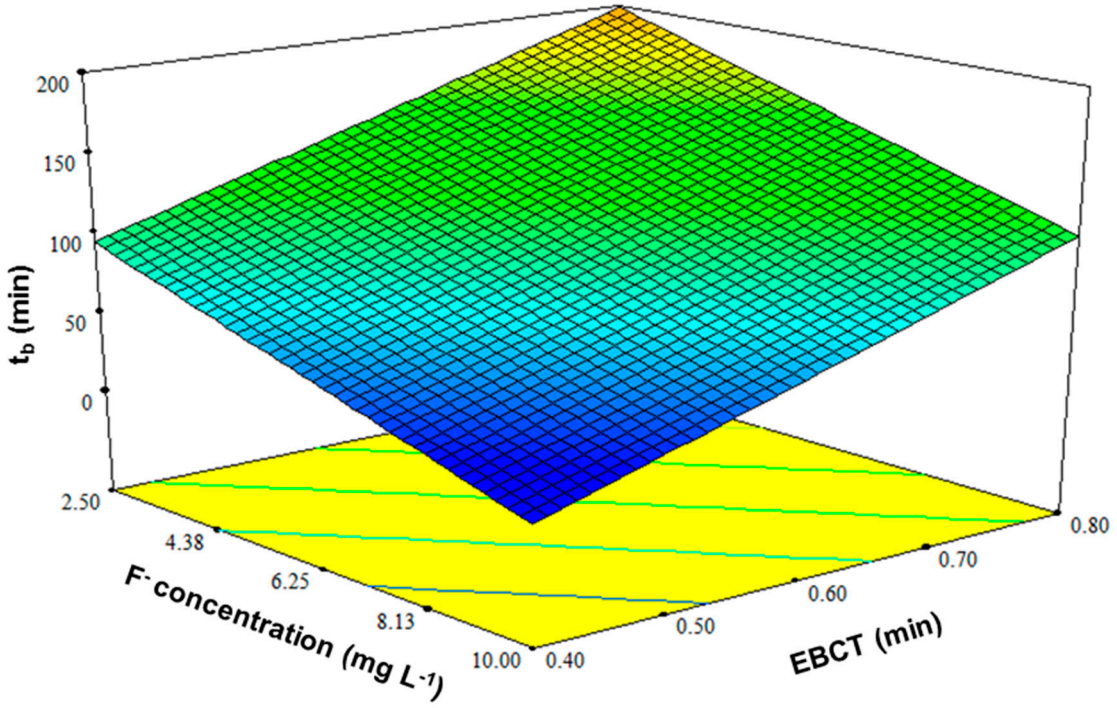

Figure 6. Variation of t_b with F^- concentration and EBCT.

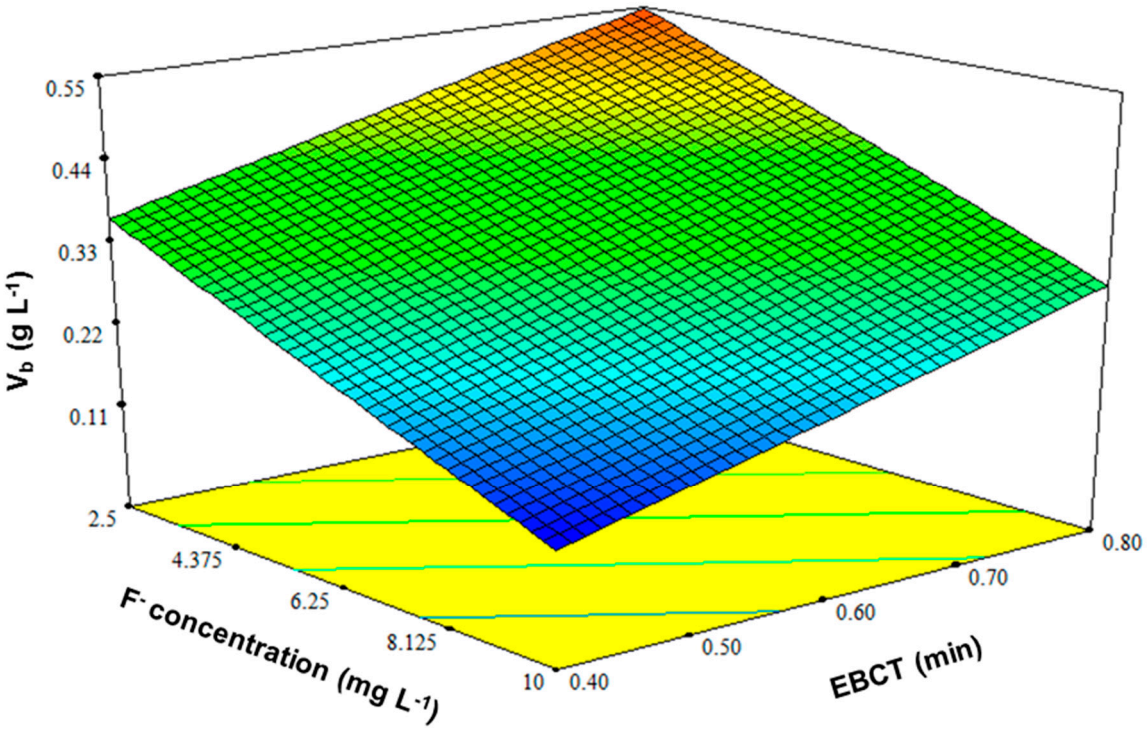

Figure 7. Variation of V_b with F^- concentration and EBCT.

Preprints (www.preprints.org) | NOT PEER-REVIEWED | Posted: 27 September 2018 doi:10.20944/preprints201809.0537.v1

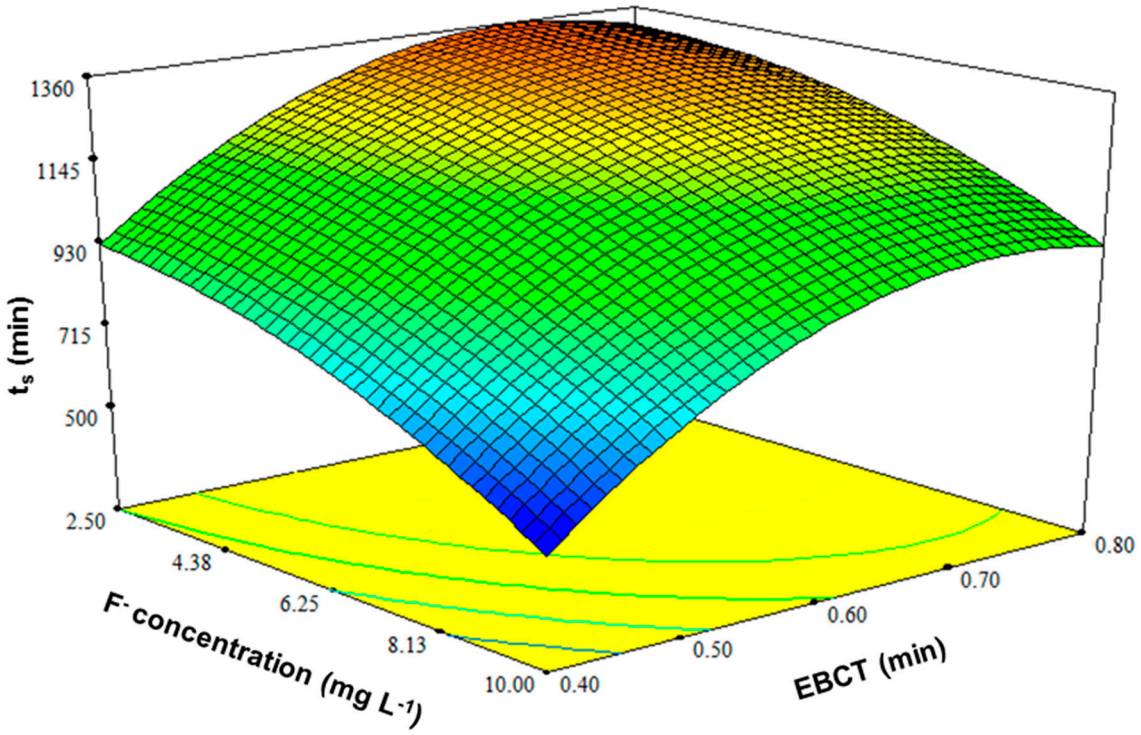

Figure 8. Variation of t_s with F^- concentration and EBCT.

3.1.4. Optimization using the desirability functions

The optimization of five objectives (F^- concentration, EBCT, t_b, V_b and t_s) was done using a multiple response method. A value that maximizes the desirability function was found through the numerical optimization. A maximum level of initial F^- concentration, minimum level of EBCT and maximum levels of response variables were established for maximum desirability. The optimized values were established to be at initial fluoride ion concentration of 4.61 mg L^{-1}, EBCT of 0.69 min, t_b of 114.75 min, V_b of 0.42 L g^{-1}, t_s of 1179.22 min and desirability of 0.511. The desirability functions were used as optimization analysis, which could be adequately applied for an adsorption process and the removal of pollutant of interest.

4. Conclusions

Material used at the present study (EMHS) is an efficient adsorbent, which can be applied to eliminate F^- and As from aqueous effluents. In column studies both fluoride ion concentration and EBCT have a significant effect on the three response variables investigated (t_b, V_b, and t_s); experimental data fits the lineal model very well. The effects of F^- concentration and EBCT on t_s is synergistic, which not can be shown by others ways, like the classical step-by-step way. The results presented demonstrate that use of surface response methodology is a potential strategy for analyzing adsorption process in adsorbent-fixed beds. A better comprehension of adsorption process will help the selection of the optimal conditions of studied variables for a given application.

Author Contributions:

C. García-Gómez and F. Almazán-García; methodology, M.L. Rivera-Huerta; software, A. Martín-Domínguez; validation, V.A. Burboa-Charis, I.C. Romero-Soto and P. Gortáres-Moroyoqui.; formal analysis, R. G. Ulloa-Mercado; writing—original draft preparation, D. Serrano-Palacios; writing—review and editing.

Conflicts of Interest: The authors declare that this article has not any financial or ethical conflict of interests.

References

1. Jadhav, S. V.; Bringas, E.; Yadav, G. D.; Rathod, V. K.; Ortiz, I.; Marathe, K. V. Arsenic and fluoride contaminated groundwaters: A review of current technologies for contaminants removal. *J. Environ. Manage.* **2015**, *162*, 306–325, doi:10.1016/j.jenvman.2015.07.020.
2. Miretzky, P.; Cirelli, A. F. Fluoride removal from water by chitosan derivatives and composites: A review. *J. Fluor. Chem.* **2011**, *132*, 231–240, doi:10.1016/j.jfluchem.2011.02.001.
3. Singh, R.; Singh, S.; Parihar, P.; Singh, V. P.; Prasad, S. M. Arsenic contamination, consequences and remediation techniques: A review. *Ecotoxicol. Environ. Saf.* **2015**, *112*, 247–270, doi:10.1016/j.ecoenv.2014.10.009.
4. Ahn, J. S. Geochemical occurrences of arsenic and fluoride in bedrock groundwater: A case study in Geumsan County, Korea. *Environ. Geochem. Health* **2012**, *34*, 43–54, doi:10.1007/s10653-011-9411-5.
5. Jadhav, S. V.; Gadipelly, C. R.; Marathe, K. V.; Rathod, V. K. Treatment of fluoride concentrates from membrane unit using salt solutions. *J. Water Process Eng.* **2014**, *2*, 31–36, doi:10.1016/j.jwpe.2014.04.004.
6. Oulebsir, A.; Chaabane, T.; Zaidi, S.; Omine, K.; Alonzo, V.; Darchen, A.; Msagati, T. A. M.; Sivasankar, V. Preparation of mesoporous alumina electro-generated by electrocoagulation in NaCl electrolyte and application in fluoride removal with consistent regenerations. *Arab. J. Chem.* **2017**, doi:10.1016/j.arabjc.2017.04.007.
7. Aoudj, S.; Drouiche, N.; Hecini, M.; Ouslimane, T.; Palaouane, B. Coagulation as a post-treatment method for the defluoridation of photovoltaic cell manufacturing wastewater. *Procedia Eng.* **2012**, *33*, 111–120, doi:10.1016/j.proeng.2012.01.1183.
8. Bansiwal, A.; Pillewan, P.; Biniwale, R. B.; Rayalu, S. S. Copper oxide incorporated mesoporous alumina for defluoridation of drinking water. *Microporous Mesoporous Mater.* **2010**, *129*, 54–61, doi:10.1016/j.micromeso.2009.08.032.
9. Yu, Z.; Xu, C.; Yuan, K.; Gan, X.; Feng, C.; Wang, X.; Zhu, L.; Zhang, G.; Xu, D. Characterization and adsorption mechanism of ZrO2mesoporous fibers for health-hazardous fluoride removal. *J. Hazard. Mater.* **2018**, *346*, 82–92, doi:10.1016/j.jhazmat.2017.12.024.
10. Solangi, I. B.; Memon, S.; Bhanger, M. I. An excellent fluoride sorption behavior of modified amberlite resin. *J. Hazard. Mater.* **2010**, *176*, 186–192, doi:10.1016/j.jhazmat.2009.11.011.
11. Zhang, Y. X.; Jia, Y. Fluoride adsorption on manganese carbonate: Ion-exchange based on the surface carbonate-like groups and hydroxyl groups. *J. Colloid Interface Sci.* **2018**, *510*, 407–417, doi:10.1016/j.jcis.2017.09.090.
12. Grzegorzek, M.; Majewska-Nowak, K. The use of micellar-enhanced ultrafiltration (MEUF) for fluoride removal from aqueous solutions. *Sep. Purif. Technol.* **2018**, *195*, 1–11, doi:10.1016/j.seppur.2017.11.022.
13. Ergun, E.; Tor, A.; Cengeloglu, Y.; Kocak, I. Electrodialytic removal of fluoride from water: Effects of process parameters and accompanying anions. *Sep. Purif. Technol.* **2008**, *64*, 147–153, doi:10.1016/j.seppur.2008.09.009.
14. Bagastyo, A. Y.; Anggrainy, A. D.; Nindita, C. S.; Warmadewanthi Electrodialytic removal of fluoride and calcium ions to recover phosphate from fertilizer industry wastewater. *Sustain. Environ. Res.* **2017**, *27*, 230–237, doi:10.1016/j.serj.2017.06.002.
15. Akter, A.; Ali, M. H. Arsenic contamination in groundwater and its proposed remedial measures. *Int. J. Environ. Sci. Technol.* **2011**, *8*, 433–443, doi:10.1007/BF03326230.

16. Reddy, K. J.; McDonald, K. J.; King, H. A novel arsenic removal process for water using cupric oxide nanoparticles. *J. Colloid Interface Sci.* **2013**, *397*, 96–102, doi:10.1016/j.jcis.2013.01.041.
17. Ghosal, P. S.; Kattil, K. V.; Yadav, M. K.; Gupta, A. K. Adsorptive removal of arsenic by novel iron/olivine composite: Insights into preparation and adsorption process by response surface methodology and artificial neural network. *J. Environ. Manage.* **2018**, *209*, 176–187, doi:10.1016/j.jenvman.2017.12.040.
18. Lee, C. G.; Alvarez, P. J. J.; Nam, A.; Park, S. J.; Do, T.; Choi, U. S.; Lee, S. H. Arsenic(V) removal using an amine-doped acrylic ion exchange fiber: Kinetic, equilibrium, and regeneration studies. *J. Hazard. Mater.* **2017**, *325*, 223–229, doi:10.1016/j.jhazmat.2016.12.003.
19. Zhang, X.; Fang, X.; Li, J.; Pan, S.; Sun, X.; Shen, J.; Han, W.; Wang, L.; Zhao, S. Developing new adsorptive membrane by modification of support layer with iron oxide microspheres for arsenic removal. *J. Colloid Interface Sci.* **2018**, *514*, 760–768, doi:10.1016/j.jcis.2018.01.002.
20. Jia, Y.; Shi, S.; Liu, J.; Su, S.; Liang, Q.; Zeng, X.; Sciences, T. L.-A.; 2018, undefined Study of the Effect of Pyrolysis Temperature on the Cd2+ Adsorption Characteristics of Biochar. *Mdpi.Com*, doi:10.3390/app8071019.
21. Saikia, J.; Sarmah, S.; Ahmed, T. H.; Kalita, P. J.; Goswamee, R. L. Removal of toxic fluoride ion from water using low cost ceramic nodules prepared from some locally available raw materials of Assam, India. *J. Environ. Chem. Eng.* **2017**, *5*, 2488–2497, doi:10.1016/j.jece.2017.04.046.
22. Dadwhal, M.; Sahimi, M.; Tsotsis, T. T. Adsorption isotherms of arsenic on conditioned layered double hydroxides in the Presence of various competing ions. *Ind. Eng. Chem. Res.* **2011**, *50*, 2220–2226, doi:10.1021/ie101220a.
23. Liu, R.; Zhu, L.; Gong, W.; Lan, H.; Liu, H.; Qu, J. Effects of fluoride on coagulation performance of aluminum chloride towards Kaolin suspension. *Colloids Surfaces A Physicochem. Eng. Asp.* **2013**, *421*, 84–90, doi:10.1016/j.colsurfa.2012.12.047.
24. Streat, M.; Hellgardt, K.; Newton, N. L. R. Hydrous ferric oxide as an adsorbent in water treatment. Part 3: Batch and mini-column adsorption of arsenic, phosphorus, fluorine and cadmium ions. *Process Saf. Environ. Prot.* **2008**, *86*, 21–30, doi:10.1016/j.psep.2007.10.009.
25. Tang, Y.; Wang, J.; Gao, N. Characteristics and model studies for fluoride and arsenic adsorption on goethite. *J. Environ. Sci.* **2010**, *22*, 1689–1694, doi:10.1016/S1001-0742(09)60307-7.
26. Kumar, N. S.; Goel, S. Factors influencing arsenic and nitrate removal from drinking water in a continuous flow electrocoagulation (EC) process. *J. Hazard. Mater.* **2010**, *173*, 528–33, doi:10.1016/j.jhazmat.2009.08.117.
27. Phillips, D. H.; Sen Gupta, B.; Mukhopadhyay, S.; Sen Gupta, A. K. Arsenic and fluoride removal from contaminated drinking water with Haix-Fe-Zr and Haix-Zr resin beads. *J. Environ. Manage.* **2018**, *215*, 132–142, doi:10.1016/j.jenvman.2018.03.018.
28. Chubar, N. New inorganic (an)ion exchangers based on Mg-Al hydrous oxides: (Alkoxide-free) sol-gel synthesis and characterisation. *J. Colloid Interface Sci.* **2011**, *357*, 198–209, doi:10.1016/j.jcis.2011.01.098.
29. Li, W.; Cao, C.-Y.; Wu, L.-Y.; Ge, M.-F.; Song, W.-G. Superb fluoride and arsenic removal performance of highly ordered mesoporous aluminas. *J. Hazard. Mater.* **2011**, *198*, 143–50, doi:10.1016/j.jhazmat.2011.10.025.
30. Tian, Y.; Wu, M.; Liu, R.; Wang, D.; Lin, X.; Liu, W.; Ma, L.; Li, Y.; Huang, Y. Modified native cellulose fibers-A novel efficient adsorbent for both fluoride and arsenic. *J. Hazard. Mater.* **2011**, *185*, 93–100, doi:10.1016/j.jhazmat.2010.09.001.
31. Chen, R.; Zhang, Z.; Yang, Y.; Lei, Z.; Chen, N.; Guo, X.; Zhao, C.; Sugiura, N. Use of ferric-impregnated

volcanic ash for arsenate (V) adsorption from contaminated water with various mineralization degrees. *J. Colloid Interface Sci.* **2011**, *353*, 542–548, doi:10.1016/j.jcis.2010.09.066.

32. Saikia, R.; Goswami, R.; Bordoloi, N.; Senapati, K. K.; Pant, K. K.; Kumar, M.; Kataki, R. Removal of arsenic and fluoride from aqueous solution by biomass based activated biochar: Optimization through response surface methodology. *J. Environ. Chem. Eng.* **2017**, *5*, 5528–5539, doi:10.1016/j.jece.2017.10.027.
33. Mollah, M. Y. a; Morkovsky, P.; Gomes, J. a G.; Kesmez, M.; Parga, J.; Cocke, D. L. Fundamentals, present and future perspectives of electrocoagulation. *J. Hazard. Mater.* **2004**, *114*, 199–210, doi:10.1016/j.jhazmat.2004.08.009.
34. Hai, F.; Yamamoto, K.; Jegatheesan, J. Special Issue on Wastewater Treatment and Reuse Technologies. *Appl. Sci.* **2018**, *8*, 695, doi:10.3390/app8050695.
35. Garcia-Gomez, C.; Rivera-Huerta, M. L.; Almazan-Garcia, F.; Martin-Dominguez, A.; Romero-Soto, I. C.; Burboa-Charis, V. A.; Gortares-Moroyoqui, P. Electrocoagulated Metal Hydroxide Sludge for Fluoride and Arsenic Removal in Aqueous Solution: Characterization, Kinetic, and Equilibrium Studies. *Water Air Soil Pollut.* **2016**, doi:10.1007/s11270-016-2783-5.
36. Li, K.; Wu, G.; Wang, M.; Zhou, X.; Wang, Z. Efficient Removal of Lead Ions from Water by a Low-Cost Alginate-Melamine Hybrid Sorbent. *Appl. Sci.* **2018**, *8*, 1518, doi:10.3390/app8091518.
37. Vijayakumar, R.; Abd Gani, S.; Zaidan, U.; Halmi, M. Optimization of the Antioxidant Potentials of Red Pitaya Peels and Its In Vitro Skin Whitening Properties. *Appl. Sci.* **2018**, *8*, 1516, doi:10.3390/app8091516.
38. Pereira, P. M.; Ferreira, B. F.; Oliveira, N. P.; Nassar, E. J.; Ciuffi, K. J.; Vicente, M. A.; Trujillano, R.; Rives, V.; Gil, A.; Korili, S.; de Faria, E. H. Synthesis of zeolite A from metakaolin and its application in the adsorption of cationic dyes. *Appl. Sci.* **2018**, *8*, doi:10.3390/app8040608.
39. Ruan, W.; Shi, X.; Hu, J.; Hou, Y.; Fan, M.; Cao, R.; Wei, X. Modeling of Malachite Green Removal from Aqueous Solutions by Nanoscale Zerovalent Zinc Using Artificial Neural Network. *Appl. Sci.* **2017**, *8*, 3, doi:10.3390/app8010003.